Statistical analysis of reduced pair correlation functions of capillaries in the prostate gland

Torsten Mattfeldt[1], **Stefanie Eckel**[2], **Frank Fleischer**[2,3], **Volker Schmidt**[2]

[1]Department of Pathology, University of Ulm, Ulm
[2]Department of Stochastics, University of Ulm, Ulm
[3]Department of Applied Information Processing & Department of Stochastics, University of Ulm, Ulm

Keywords: Angiogenesis, bootstrap, capillary, computer-intensive methods, fibre process, K-function, microscopy, pair correlation function, point processes, spatial statistics, stochastic geometry.

Running title: Statistical analysis of second-order properties of capillaries

Address for correspondence: Prof. Dr. T. Mattfeldt, Department of Pathology, Oberer Eselsberg M23, D-89081 Ulm, Germany. E-mail: torsten.mattfeldt@medizin.uni-ulm.de Fax: ++49 731 50 23384

Abstract

Blood capillaries are thread-like structures that may be considered as an example of a spatial fibre process in 3D. At light microscopy, the capillary profiles appear as a planar point process on sections. It has recently been shown that the observed pair correlation function $g(r)$ of the centres of the fibre profiles on two-dimensional sections may be used to estimate the reduced pair correlation function of stationary and isotropic fibre processes in 3D (Krasnoperov & Stoyan, 2004). In the present paper, it was explored how this approach may be extended to statistical analysis of reduced g-functions of capillaries from multiple specimens of different groups and with replicated observations. The methods were applied to normal prostatic tissue compared to prostate cancer. Confidence intervals for the mean reduced g-functions of groups were estimated for fixed r-values parametrically using the t-distribution, and by bootstrap methods. Each estimated reduced g-function was furthermore characterized in terms of its first maximum and minimum. The mean length of capillaries per unit tissue volume was significantly higher in prostate cancer tissue than in normal prostate tissue. Significant differences between the mean reduced g-functions of malignant and benign lesions could be demonstrated for two domains of r-values. Bootstrap-based confidence interval were slightly wider than parametrically estimated confidence intervals, in general. Falsely negative lower bounds of the intervals, which sometimes arose using the parametric approach, could be avoided by the bootstrap method. Testing of group mean values for significant differences by the bootstrap method yielded more conservative results than multiple t-tests. The functional value of the first maximum of the reduced g-function and a global statistical parameter of short-range ordering were significantly reduced in the carcinoma group. Prostate cancer tissue is more densely supplied with capillaries than normal prostate tissue, and the three-dimensional arrangement of the vessels differs with respect to interaction at various distance ranges. In the local approach used here, bootstrap methods can be used as a robust statistical tool for the computation of confidence intervals and group comparisons of mean reduced g-functions at specific ranges of interaction.

1 Introduction

Blood vessels have two basic functions: blood transport between the heart and the tissues, and exchange of blood constituents between tissue and blood (oxygen, carbon dioxide, molecules arising in cell metabolism, ...). While all blood vessels such as arteries, arterioles, capillaries, venoles and veins are involved in blood transport, the exchange of constituents between blood and tissues is largely restricted to the smallest, hairlike peripheral vessels of the body: the blood capillaries. They are defined as blood vessels whose wall consists only of endothelial cells and a basement membrane (Mattfeldt & Mall, 1984). In the capillaries, the diffusion distance for the transported molecules is minimal. The density of capillarization is an important factor for the oxygen supply of a tissue. The denser the capillary network, the shorter is the mean diffusion distance for oxygen. Hence organs with very high oxygen consumption such as the heart muscle possess an extraordinarily dense capillary network (Mattfeldt & Mall, 1984).

In the process of the development of a neoplasm, the growing tumour tissue needs to be supplied with new capillaries, after it has reached a certain critical size. The growth of new vessels in general is denoted as angiogenesis. Capillary angiogenesis in tumors is a topic of central importance in tumour biology. In the exploration of mechanisms of angiogenesis, the basic structural background remains the capillary network itself, which can be visualized by microscopy. At least in the light microscope, tumour capillaries look largely identical to normal capillaries. Hence a qualitative, descriptive approach does not provide enough information when comparing the capillary supply of different tumours, or when comparing the capillarization of untreated tumours and tumours treated by drugs or radiation. To obtain objective findings in such investigations, it is obligatory to quantify the capillarization. For this purpose methods of quantitative stereology are relevant (Mattfeldt & Mall, 1984; Mattfeldt et al., 2004a, b). These methods are rooted in the mathematical domain of stochastic geometry, where capillaries may be considered as an example of a 3D fibre process.

Fibre processes are random geometrical models for fibrous structures. They are used in applications in biology, medicine and material science, for example (Mattfeldt et al., 1994; Stoyan et al., 1995; Krasnoperov &

Stoyan, 2004). Fibres may be intuitively defined as thread-like structures, i.e. filamentous or thin tubular structures whose length greatly exceeds their width. After cutting, such fibres appear on a microscopic section as dots, e.g. small ellipses when the true fibres are circular or elliptical cylinders. In the case of isotropic and stationary capillary networks, three simple first-order parameters can be estimated by using information from sections of arbitrary location and orientation by using elementary stereological equations:

$$V_V = A_A \tag{1.1}$$

$$S_V = (4/\pi) B_A \tag{1.2}$$

$$L_V = 2 Q_A \tag{1.3}$$

(see e.g. Weibel, 1989; Mattfeldt et al., 1990; Mattfeldt et al., 2004a,b; Howard & Reed, 2005). Here the stereological shorthands denote: V_V: the volume of capillaries per unit reference volume; A_A: the area of capillary profiles per unit reference area on sections; S_V: the surface area of capillaries per unit reference volume; B_A: the boundary area of capillary profiles per unit reference area on sections; L_V: the length of capillaries per unit reference volume, i.e. the intensity of the 3D fibre process; Q_A: the number of capillary profiles per unit reference area on sections. The three parameters on the left side of eqs. (1.1)-(1.3) express the density of capillary supply in 3D space in different terms. Among these, eq. (1.3) is the most important, because L_V is the intensity of the fibre process itself, and does not depend on the fibre thickness (capillary diameter). In applications, often the stereological extrapolation from Q_A to L_V is not explicitly performed, but only Q_A is reported as 'capillary density' or 'microvessel density' (e.g. Heimburg et al., 1999; Rubio et al., 2000; Vaquero et al., 2000; Vidal et al., 2001).

Even the exhaustive set of all three model parameters V_V, S_V and L_V does not provide a complete geometrical characterization of a capillary network. The first-order parameters tell nothing about the geometrical architecture (pattern) of the blood vessels, i.e. their spatial arrangement relative to each other. To describe arrangements of random sets in space, a well-established approach consists in methods of second-order stereology. Such techniques have hitherto been used mostly for random sets with positive volume fraction (volume processes) (Cruz-Orive, 1989;

Mattfeldt et al., 1993, 1996; Mattfeldt & Stoyan, 2000; Mattfeldt et al., 2000; Mattfeldt, 2003). In principle, however, they may also be used for the second-order characterization of surface processes and fibre processes in 3D space (Mattfeldt et al., 1994; Stoyan et al., 1995). In a recent paper, it was shown how second-order stereological inference on isotropic spatial fibre processes may be performed on the basis of observations on two-dimensional sections (Krasnoperov & Stoyan, 2004). The ordinary planar pair correlation function $g(r)$ of the sectional profiles of the fibres can be used to estimate the reduced pair correlation function $g_3(r)$ of the 3D fibre process (Krasnoperov & Stoyan, 2004). In this methodological paper, the emphasis was put on point estimation of the reduced pair correlation function. However, in an experimental or clinical research project with more data, it is desired to provide confidence intervals of the function for groups of cases, and to test for significant differences between groups. Such an attempt at statistical inference was made in the present paper. For this purpose, one of the most elementary questions was addressed: How does the capillary architecture of normal tissue deviate from the capillary architecture of cancerous tissue from the same organ? This question was studied for one of the most frequent malignant tumours of man: prostate cancer (Mattfeldt et al., 2004a,b). Motivated by a previous study (Mattfeldt & Fleischer, 2005), two approaches were used in comparison: classical statistical inference methods relying on the assumptions of normality and homoscedasticity of the data, as well as bootstrap methods as non-parametric approach.

2 Methods

2.1 Explorative statistical analysis of planar point patterns

After digitizing the coordinates of the midpoints of the fibre profiles on sections, exploratory methods of data analysis can be applied to characterize the 2D point process of the fibre profile midpoints. The most basic information is an estimate of the *intensity* λ of the point process, i.e. the mean ($= E =$ expected) number of points per unit reference area. Recall that if $X = \{X_n\}$ is a motion-invariant point process and W is a sampling window then

$$\lambda = \frac{E(X(W))}{|W|}, \tag{2.4}$$

where $X(W)$ measures the number of points of X located in W and $|W|$ denotes the area of W. A natural estimator for the intensity λ is given by

$$\widehat{\lambda} = \frac{X(W)}{|W|}. \tag{2.5}$$

Notice that usually λ^2 is not estimated as $(\widehat{\lambda})^2$ but as

$$\widehat{\lambda^2} = \frac{X(W)(X(W)-1)}{|W|^2} \tag{2.6}$$

(Stoyan & Stoyan, 1994, p. 277). While the intensity is a single quantity, second-order functions (summary statistics) provide a series of values as a function of the interpoint distance r. Their functional values indicate which kind of interaction between points prevails at a certain distance. This interaction may consist in attraction (clustering) or repulsion, or otherwise there may be no interactive effects between the points at all at a certain distance. For the estimation of the summary statistics it is advisable to rely on stationarity and isotropy as mathematical model assumptions. In practice, isotropy means lack of a preferred orientation of the points. Stationarity implies that there are no systematic gradients of the point density, and that all areas of the reference space potentially may contain points. Images evaluated for point process statistics must not have 'black holes' due to artifacts.

One of the most popular functions of explorative spatial point pattern analysis is Ripley's *K-function* $K(r)$ (reduced second moment function) (Ripley, 1988; Stoyan et al., 1995). Intuitively, $K(r)$ is the mean number of other points of the process lying within a circle of radius r, centred about a typical point (x, y) of the process, divided by the intensity of the process:

$$K(r) = \frac{E(\text{number of other points of X with distance} \leq r \mid \text{X has point at } (x,y))}{\lambda} \tag{2.7}$$

where the symbol '|' denotes 'conditional to'. Notice that the conditioning here is not to be regarded in a strict mathematical sense since

the probability for a stationary point process X to have a point in a particular location (x, y) equals 0. More formally one can define $K(r)$ for a motion-invariant point process $X = \{X_n\}$ as

$$K(r) = E \sum_{X_n \in W} \frac{X(b(X_n, r)) - 1}{\lambda^2 |W|}, \tag{2.8}$$

where $b(X_n, r)$ is the disc around X_n with radius r. The concept of a typical point of the process means that a point is selected from all points of the process at random with uniform probability. It has to be contrasted against the concept of a uniform random point in the xy-plane where all points (and not just those of the process) are considered. In the evaluation of $K(r)$, the typical point itself, i.e. the centre of the circle in which the points are counted, is not counted, hence the word 'other' in the definition of $K(r)$ above. The estimation of $K(r)$ has to be performed using edge-corrected estimators as described e.g. in Diggle (2003) and in Stoyan & Stoyan (1994). In particular we used

$$\widehat{K}(r) = \frac{\kappa(r)}{\widehat{\lambda^2}}, \tag{2.9}$$

where

$$\kappa(r) = \sum_{\substack{X_i, X_j \in W \\ i \neq j}} \frac{1_{b(o,r)}(X_j - X_i)}{|W_{X_j} \cap W_{X_i}|}, \tag{2.10}$$

and $W_{X_j} = \{x + X_j : x \in W\}$ is the set W translated by the point X_j. Notice that the usage of the denominator ensures edge-correction. Often instead of $K(r)$ the function $L(r)$ given by

$$L(r) = \sqrt{\frac{K(r)}{\pi}} \tag{2.11}$$

is regarded.

As reference model (null hypothesis) for isotropic and stationary point processes, the model of a stationary Poisson point process is used. In this case there is no interaction between the points at all distances and the number of points in a sampling window W is Poisson distributed with parameter equal to the intensity λ of the Poisson point process times the area of W. The points are distributed independently at random, isotropically and homogeneously in the plane, a state which has

rightfully been denoted as complete spatial randomness of points (CSR) (Diggle et al., 1991, 2000; Schladitz et al., 2003). It is easy to see that under these conditions, a circle with radius r around a typical point of a Poisson point process contains $\lambda\pi r^2$ points on the average, namely the product of the area of the circle and the intensity. After division of this value by λ, one obtains the K-function for the planar Poisson point process:

$$K^{Poi}(r) = \pi r^2. \tag{2.12}$$

An initial curve segment with $K(r) = 0$ indicates that the interpoint distance does not attain values below a certain minimum. In the case of biological structures such as cells, cell nuclei or capillaries, this behaviour may simply result from their physical size, if no overlapping is possible. Such curve segments may hence be interpreted as a sign of a hard-core property. The lowest r-value for which the sample K-function reaches a positive value, r_0, may be considered as an estimate of the hard-core distance.

In analogy to a probability density function, which is the derivative of a cumulative distribution function, there is a counterpart to the K-function, namely *the pair correlation function* $g(r)$, which may be obtained after differentiation and normalization of $K(r)$:

$$g(r) = \frac{1}{2\pi r}\frac{dK(r)}{dr}. \tag{2.13}$$

In the case of a planar Poisson point process, we obtain

$$g^{Poi}(r) \equiv 1 \tag{2.14}$$

for all r (by insertion of $K(r) = \pi r^2$ into eq. (2.13)). Values of $g(r)$ below 1 indicate repulsion, values above 1 indicate clustering for point pairs of such a distance r. A hard-core effect leads to an initial segment with zero values of $g(r)$. Similar to a probability density function, hills and valleys above and below the constant value 1 indicate domains of r-values with tendencies of the points for aggregation and repulsion, respectively. The pair correlation function may also be defined as the product density of second order of the point process, divided by the square of the intensity for the purpose of normalization (Stoyan & Stoyan, 1994, p. 249; Stoyan et al., 1995, p. 129). Hence an estimator for $g(r)$ is given by

$$\widehat{g}(r) = \frac{\widehat{\varrho^{(2)}}(r)}{\widehat{\lambda}^2}, \tag{2.15}$$

where

$$\widehat{\varrho^{(2)}}(r) = \frac{1}{2\pi r} \sum_{\substack{X_i, X_j \in W \\ i \neq j}} \frac{k_h(r - ||X_i - X_j||)}{|W_{X_i} \cap W_{X_j}|} \tag{2.16}$$

is an estimator for $\varrho^{(2)}(r)$, the product density of second order. For the estimator $\widehat{\varrho^{(2)}}(r)$, similarly to the estimator for $K(r)$, the denominator $|W_{X_i} \cap W_{X_j}|$ ensures edge-correction. Notice that $k_h(x)$ denotes the Epanechnikov kernel

$$k_h(x) = \frac{3}{4h}(1 - \frac{x^2}{h^2}) 1_{(-h,h)}(x), \tag{2.17}$$

and that we used a corresponding bandwidth $h = 0.1/\sqrt{\widehat{\lambda}}$. For more details on the consideration of edge effects see Ripley (1988), Stoyan et al. (1995), and Diggle (2003).

2.2 Second-order statistics of spatial fibre processes

In a recent paper it was shown that in the context of fibre processes, an additional stereological interpretation of the observed K-function and the observed pair correlation function $g(r)$ of the profile midpoints is possible (Krasnoperov & Stoyan, 2004). Let us denote the intensity of the fibre process as L_V (mean length of fibres per unit volume), as usual in stereology. Its K-function $\tilde{K}_3(r)$ is the mean length of the fibres in a sphere with radius r, centred about a typical point of the fibre process, divided by L_V. In the three-dimensional case it holds for the corresponding pair correlation function $\tilde{g}_3(r)$:

$$\tilde{g}_3(r) = \frac{1}{4\pi r^2} \frac{d\tilde{K}_3(r)}{dr} \tag{2.18}$$

It was shown that a 'reduced variant' $g_3(r)$ of $\tilde{g}_3(r)$ can be estimated from sections if its definition is adapted in the spirit of the definition of the pair correlation function of a planar point process. Remember that in this setting only the number of 'other' points of the process is counted in circles around typical points, but the typical point itself is

not counted. In analogy, the *reduced K-function* $K_3(r)$ may be defined as the expected length of the 'other' fibres in a sphere of radius r centred at a typical point of the fibre process, whereby the length of the fibre running through the typical point itself is not counted, divided by L_V. Then, having in mind eq. (2.18) and by replacing $\tilde{K}_3(r)$ with $K_3(r)$, the reduced pair correlation function $g_3(r)$ can be defined as

$$g_3(r) = \frac{1}{4\pi r^2} \frac{dK_3(r)}{dr} \tag{2.19}$$

In Krasnoperov & Stoyan (2004) estimators for $g_3(r)$ of the form

$$\widehat{g}_3(r) = \widehat{g}(r) \tag{2.20}$$

are suggested. For practice, this result means: the estimator $\widehat{g}(r)$ considered in eq. (2.15) for the ordinary planar pair correlation function $g(r)$ of the sectional profiles of the fibres is an estimator of the reduced pair correlation function $g_3(r)$ of the 3D fibre process. As model requirements, it is necessary to assume isotropy and stationarity of the fibre process. This state has previously been denoted as 'complete directional randomness' (Mattfeldt et al., 1994).

Null models for spatial fibre processes are a Poisson line process and a Boolean segment process in 3D (Stoyan et al., 1995, p. 83, p. 250). They represent complete spatial randomness of lines or line segments in space, respectively, just as a Poisson point process represents CSR of points. At CSR of a 3D fibre process we have $K_3^{Poi}(r) = (4\pi/3)r^3$. Hence with eq. (2.19) it follows $g_3^{Poi}(r) = 1$ at CSR for the 3D fibre process for all r (Krasnoperov & Stoyan, 2004). Thus, the criteria for evaluation of the $\widehat{g}_3(r)$-curves from empirical data remain essentially the same as those for $\widehat{g}(r)$ in the planar case. Values below 1 indicate repulsion, and values above 1 indicate clustering. In its first application (Krasnoperov & Stoyan, 2004), the new estimator was used to investigate blood capillaries in normal rat thyroid glands. The main requirements of isotropy and stationarity should hold in first approximation for many biological fibre processes, e.g. for capillaries in glandular tissues and in many tumour tissues. The hard-core distance of the point process of the fibre profiles on sections may be interpreted in 3D as the minimal distance between the longitudinal axes of the capillaries.

2.3 Statistical methods

2.3.1 Bootstrap methods

The bootstrap method was developed by Efron in 1979 and consists basically in an independent random resampling of the sample data with replacement (Efron & Tibshirani, 1993; Ludbrook, 1995). It is a computer-based method largely free of statistical model assumptions. Typically, from 100–10000 bootstrap samples an arbitrary statistic of interest (the *bootstrap statistic)* is computed. It is assumed that the distribution of the bootstrap statistics (usually denoted as D^*) approximates the distribution of the statistic D in the population. The bootstrap belongs to the *computer-intensive resampling methods;* other pertinent examples are *jackknife techniques, permutation and randomization tests* (Efron & Tibshirani, 1993; Ludbrook, 1995).

Up to now, bootstrap methods have been exploited in stereology only scarcely. They have been used in the context of point process statistics (Diggle et al., 1991, 2000; Schladitz et al., 2003) and recently for statistical inference from stereological estimates of volume fraction (Mattfeldt & Fleischer, 2005). Using the bootstrap method, it is possible to provide statistical inference from sets of independent data (e.g. a single estimate of V_V per case), or from a series of dependent data (e.g. an estimated K-function of a series of r-values per case; see Diggle et al., 1991, 2000; Schladitz et al., 2003).

2.3.2 Confidence intervals

An estimate $\widehat{g}^{(i)}(r)$ of the $g(r)$-function at a given r-value in the i'th case of n cases was obtained as the arithmetic mean of the values of the two estimated $g(r)$-functions resulting from two images per case. To estimate a parametric 95% confidence interval for $g(r)$ for a group of n cases, the following statistic standard procedure was used. Let us denote the mean of the $\widehat{g}^{(i)}(r)$-values from the n cases for fixed r as

$$\bar{\widehat{g}}(r) = \frac{1}{n}\sum_{i=1}^{n}\widehat{g}^{(i)}(r). \tag{2.21}$$

If the assumption of a Gaussian distribution of the data is fulfilled, estimates of the bounds of a 95% confidence interval for this mean value are

given by $(\bar{\widehat{g}}(r) \pm t_{0.975,n-1} SE(\bar{\widehat{g}}(r)))$, where $t_{0.975,n-1}$ is the quantile of the t-distribution used for a 95% confidence interval for $(n-1)$ degrees of freedom (see Howard & Reed, 2005, p. 151). To obtain a bootstrap confidence interval for $g(r)$, we created 1000 bootstrap samples $S_1, ..., S_{1000}$ with n items from the original sample $S_{orig} = \{\widehat{g}^{(1)}(r), ..., \widehat{g}^{(n)}(r)\}$, where in this case $n = 12$. The sampling is independent and with replacement. For all 1000 bootstrap samples their corresponding mean values

$$D_i^* = \frac{1}{n} \sum_{j=1}^{n} \widehat{g}^{(i,j)}(r) \tag{2.22}$$

are computed, where $\widehat{g}^{(i,}j)(r)$ denotes the jth item in S_i. The 1000 values D_1^*,..,D_{1000}^* are sorted by size. The lower and upper bounds of a 95%-confidence interval of $\bar{\widehat{g}}(r)$ were estimated by the 26th and the 975th value of D^* in this sequence (Mattfeldt & Fleischer, 2005).

2.3.3 Significance tests

As parametric test for a significant difference between the mean values of $g(r)$ from two groups A and B with $n_A = 12$ and $n_B = 12$ cases, the classical two-sample t-test (Student's t-test) was used. The bootstrap test statistic D for the two samples was computed as the difference of the sample means $\bar{\widehat{g}}_A$ and $\bar{\widehat{g}}_B$: $D = \bar{\widehat{g}}_A - \bar{\widehat{g}}_B$. For the generation of bootstrap samples, the two samples were united to a common sample of size $n_A + n_B = 24$. From this sample, we created 999 pairs of bootstrap samples $S_i = (S_A^{(i)}, S_B^{(i)})$ with n_A and n_B items and mean values $\bar{\widehat{g}}_A^{(i)}$ and $\bar{\widehat{g}}_B^{(i)}$. The sampling is independent and with replacement. For all 999 bootstrap sample pairs, the difference D_i^* between the group mean values $\bar{\widehat{g}}_A^{(i)} - \bar{\widehat{g}}_B^{(i)}$ was computed. Finally, the D_i^*-values of the bootstrap samples and the D-value from the real sample were ordered by size. If the rank of D in this series was less than or equal to 25, or if the rank is higher than or equal to 976, the result was considered to be significant at a level of 5% (Mattfeldt & Fleischer, 2005).

2.3.4 Evaluation of individual reduced g-functions

In addition to the local computation of confidence intervals and significance tests for fixed r, each estimated reduced g-function per visual field

was evaluated with a method presented by Stoyan & Schnabel (1990) (see also Stoyan & Stoyan, 1994, pp. 250–258). This procedure includes identification of the first maximum g_{max} and the next following minimum g_{min} with the corresponding r-values r_{max} and r_{min} for each reduced g-function, where $r_{min} > r_{max}$. From these data, the statistic

$$M = \frac{g_{max} - g_{min}}{r_{min} - r_{max}} \tag{2.23}$$

was computed (Stoyan & Stoyan, 1994, p. 251). The statistic M is related to the global degree of order in the spatial point pattern. Large values indicate a high degree of order and may be expected e.g. in the case of point patterns with an element of periodicity. The statistic may be used as a tool to summarize the course of the reduced g-function by a single quantity.

These evaluations provided two values of each statistics per case, because two reduced g-functions were computed per case. The statistical handling of these data is not elementary. In contrast to the estimates for L_V and for $g(r)$ themselves, they represent minimum and maximum properties extracted from $g(r)$. For these data a simple arithmetic averaging might be not appropriate. For example, if the hard-core distance estimated from two images is e.g. 16 and 20 pixels, one could argue that the best estimator is 16 pixels and not 18 pixels, because the hard-core distance is a minimum property. However, this would entirely neglect the information from the second image, which seems unwise. For the summary characteristics it was finally decided to perform no averaging within cases before making significance tests between groups, but to keep both values unchanged. The significance tests were performed on the basis of $12 \times 2 = 24$ equally weighted data per group, which leads to t-tests with 47 degrees of freedom.

2.4 Practical methods

For the practical investigations, twelve routine cases of prostatic cancer in whom radical prostatectomies had been performed were chosen. These had been examined histopathologically of the Department of Pathology of the University of Ulm. As control group with normal tissue, the tumour-free regions of 12 radical prostatectomy specimens with prostatic cancer were used (Figs. 1, 2). Paraffin sections were stained

using an antibody versus CD34, a routine immunhistochemical marker for endothelial cells which is often used for the estimation of the microvessel density in tumours (Heimburg et al., 1999; Rubio et al., 2000; Vaquero et al., 2000; Vidal et al., 2001) (Fig. 2). The sections were viewed under a Zeiss Axiophot light microscope, connected to a JVC 3-CCD camera attached to a PC. About 10–15 visual fields per case were acquired and stored using the software Diskus 4.50 FireWire under Windows 2000. The technically best two images of these series were selected according to quality criteria (best staining quality of the capillaries, well preserved morphology of tissue, absence of artifacts etc.). This approach provided two rectangular visual fields per case with 1240 $\times$ 1000 pixels, in which 61–341 capillary profiles could be found per field (Fig. 3). At the final magnification, one pixel corresponded to 1.5 μm, hence fields with edgelengths 1860 μm $\times$ 1500 μm were evaluated.

The colour images were stored as TIF-files and analyzed interactively using standard imaging software under Windows NT (Adobe Photoshop, Imagetool). The centres of the capillary profiles were detected interactively (Figs. 1,2) (see also Krasnoperov & Stoyan, 2004). The coordinates of these points were stored as ASCII data sets. The reduced pair correlation function $g(r)$ was estimated for each image as described in section 2.1 at steps of 0.5 for r-values up to 500 pixels, i.e. for $r = 0, 0.5, 1, ..., 499, 499.5, 500$. The estimation of $g(r)$ was performed by using GeoStoch, a Java-based open-library system developed by the Department of Applied Information Processing and the Department of Stochastics of the University of Ulm (Mayer et al., 2004; http://www.geostoch.de). Parametric and bootstrap-based 95%-confidence intervals as well as tests on significant differences between the group mean values were computed for $r = 1, 2, ..., 99, 100$, and for $r = 100, 105, ..., 495, 500$. The hard-core distance was estimated for each visual field as the minimum value of the interpoint distances.

3 Results

3.1 Qualitative observations

Inspection of the sections immunohistochemically stained with an antibody versus CD34 disclosed numerous positively marked (brown stained) small dotlike areas (Figs. 1a, 2a). Dependent on the direction of cutting,

these varied from elliptical to circular shape. These dots were checked exemplarically by comparison with the usual Haematoxylin-Eosin stain from the same areas. It was found that all CD34-positive areas in normal prostatic tissue and prostatic cancer tissue were morphologically consistent with blood vessels. Sometimes a few larger vessels such als venoles were stained in addition to the largely preponderant capillaries, too, but these were easily discernible from capillaries by their thicker walls. In all cases, the capillaries lay only within the stromal parts of normal and neoplastic prostatic tissue, i.e. they were always surrounded at least by a thin rim of connective tissue and were never directly enclosed by epithelial cells. Often the capillaries were found near the borders between glandular lumina and adjacent stroma fields (Figs. 1b, 2b). No preferential directions of the points were visible in both classes of specimens (Figs. 1b, 2b). By visual inspection alone, it was not possible to detect clear differences between the point patterns of capillary profiles in normal and neoplastic tissue.

3.2 Individual reduced g-functions

Fig. 4 shows the plots of selected individual reduced g-functions from both groups. Invariably the curves began with a flat curve segment and thereafter attained positive values, usually quickly mounting to a first maximum g_{max} and then descending to a first minimum g_{min} (Figs. 4a,b). Visual inspection of the individual plots showed no clear qualitative difference between the reduced g-functions for normal and cancerous tissue.

3.3 Mean values of groups

First of all, it was found that the mean intensity of the capillary fibre process, L_V, was increased in the prostatic cancer group by 47% as compared to tumour-free tissue ($p < 0.01$) (Table I). For the further statistical evaluations, estimates of the mean reduced g-functions per group were obtained, and 95% confidence intervals were computed by classical and bootstrap methods. Selected results are shown in Table II. Bootstrap-based confidence intervals computed with 1000 bootstrap samples per r-value lay globally in the same order of magnitude as classically computed confidence intervals. However, the bootstrap intervals

were slightly wider than the classically estimated confidence intervals, in general. For low r-values, which led to very small g-values near 0 in both groups (see Table II for $r = 3$–6 pixels in the normal group and for $r = 3$–7 pixels in the carcinoma group), application of the parametric standard formula for computation of interval bounds led to negative lower bounds (Table II). In contrast, bootstrapping provided positive lower bounds also in these domains (Table II). The mean reduced g-functions of the two groups are plotted with bootstrap confidence intervals in Figs. 5a,b.

To test for statistical differences between the mean reduced g-functions at fixed r-values, multiple t-tests and bootstrap tests were performed. The results are shown in Table III and Fig. 5c. Significant differences between the group mean values of $g(r)$ were found according to the bootstrap method for the ranges of $r = 10$–32 and $r = 64$–69 pixel. In both domains, the g-values were significantly reduced in the carcinoma group. The outcomes of the bootstrap tests were slightly more conservative than the outcomes of multiple t-tests, which yielded significant differences in the ranges $r = 9$–40 pixels and $r = 60$–77 pixels.

3.4 Summary characteristics of reduced g-functions

Using the methods decribed in section 2.3.3, the summarizing characterics r_{max}, g_{max}, r_{min} and g_{min} were computed for all individual reduced g-functions. From these values the statistic M was computed (Stoyan & Schnabel, 1990; Stoyan & Stoyan, 1994). The minimum interpoint distance was also recorded for each reduced g-function. The results are shown in Table I. For the sake of simplicity only the results for Student's t-test are presented; bootstrap tests led to the same conclusions. There was no significant difference between the mean hard-core distances of the two groups. However, there was a highly significant decrease of mean g_{max} in the cancer group. This finding led to a significant decline of the statistic M. There were no significant differences between group means with respect to r_{max}, r_{min}, and g_{min}. Summarizing, these data corroborate the finding that capillary patterns of normal and neoplastic prostatic tissue are spatially different, which was also concluded on the basis of the r-wise comparison of the mean reduced g-functions.

4 Discussion

4.1 Discussion of capillary changes after neoplastic transformation

The main results of the present study may be summarized as follows. Compared with normal prostatic tissue, the capillary length density is significantly increased in prostatic cancer. Using classical and bootstrap inference methods for r-wise comparisons of mean g-values, a significant decrease of the mean g-values at various distances could be demonstrated in the prostatic cancer group. Parallel to this change, it could be shown that the height of the first maximum of the pair correlation function declined in the carcinoma group. For an interpretation of the changes of the second-order properties, the following considerations seem appropriate. i) The increase of the intensity L_V of capillaries in the cancer group was not accompanied by a diminished hard-core distance in the cancerous group, which might be expected. ii) It cannot be excluded that the second-order changes are partially due to a higher intensity of the capillaries in the carcinoma group. For the simple case of a Poisson process, the pair correlation function is not affected by the density of the points; we have $g(r) \equiv 1$ for the Poisson process irrespectively of the intensity. However, here we are faced with hard-core point processes. Under this condition second-order statistics such as $g(r)$ may well be influenced by the intensity. To study this question in more depth, it would be informative to perform simulation studies with hard-core point processes of different intensities and with the same hard-core distance, and to compare the resulting reduced g-functions. iii) Another explanation for the observed alterations of the reduced g-function is a true change of the inner order of the neoplastic tissue as compared to the normal tissue that affects the capillary arrangement, irrespectively of the intensity of the process. An important clue may lie in the observation that the capillaries were found only within the stroma and never within the epithelium, and that the capillaries were often located near the outer surfaces of the epithelial building blocks (see Figs. 1, 2). After completing the studies on the capillaries, the volume fractions of stroma in the two groups were estimated by point counting with 150 points per image. It was found that the volume fraction of stroma was $\approx 44\%$ in the normal group and $\approx 50\%$ in the carcinoma group; the difference was

not significant. Hence simple alterations of the volume fraction of the stroma seem not to be responsible for the observed capillary changes. A possible explanation could, however, consist in the geometry of the individual glands in normal and cancerous tissue. In normal tissue one usually finds complexes of relatively small glands (the normal lobules) (Fig. 1). Carcinomas show much larger glands, in particular those with poor differentiation (the cribriform type), whereas the small lobules get lost (Fig. 2). As the capillaries tend to surround the glands, this leads to a preponderant clustering at shorter distances in the normal tissue. In carcinomas, an inhibition of capillary clustering at short distances has to be expected due to the loss of the normal lobules. Moreover, it could be seen that thin stromal septa containing capillaries often arise in carcinomatous tissue, which reach deeply into the glands (see Fig. 2). These septae also may lead to a partial loss of clustering of the capillaries around the glands, which is typical for the normal tissue. All the aforementioned factors could contribute to the decrease of $g(r)$ for some r-values in the carcinoma group as compared to the normal tissue.

4.2 Stereology of capillaries: general aspects

Up to now we have discussed the nature of the change in capillarization after transition from normal to neoplastic prostatic tissue. A more elementary question is to ask for the nature of the two point processes, each viewed separately from the viewpoint of exploratory statistics. A first step could be a check whether the observed point patterns are compatible with a planar Poisson point process by a Monte-Carlo test on CSR (Schladitz et al., 2003; Baddeley & Turner, 2005). Here such tests were not performed, because it was obvious at first sight that the observed point processes were not compatible with planar Poisson point processes. They are clearly hard-core point processes. An informative approach would consist in a stochastic modelling of the observed point processes. An obvious way towards modelling could consist in parameter fitting on the basis of a known stochastic point process model, which must take into account the hard-core property in the first instance (Baddeley & Turner, 2005). Similar as in our previous investigation on point processes of intramembranous particles, the initial repulsive pattern was followed by clustering of the points at longer distances (see Schladitz et al., 2003, Figs. 4–6). Here one could consider for example

a Gibbs model (Stoyan & Stoyan, 1994; Stoyan et al., 1995; Schladitz et al., 2003). An attractive alternative idea is statistical reconstruction of the point process. Instead of using a parametric model, one proceeds from extracted data of the empirical images itself. For example, the intensity and second-order functions of the observed point process are estimated from the images, and simulations of point processes are then performed conditional to these data. Reconstruction methods were extensively applied in the domain of random sets, see the work of Torquato and coworkers (Yeong & Torquato, 1998; Manwart et al., 2000; Torquato, 2001). For point processes they have only scarcely been used (Tscheschel & Stoyan, 2005). If the reconstruction is successful, one obtains additional simulated images with a point process with nearly the same properties as the observed one. Concatenation of these images yields then a virtually enlarged visual field without further microscopical overhead. In principle, this technique would also be applicable to the sets of capillary profile coordinates obtained in this study.

The observation that capillaries lie only in the stroma and never inside the epithelium has the following consequences. In the end, it means that the capillaries cannot originate from all parts of the total reference space, i.e. the total tissue, but only from a subset of it, i.e. the stroma. Hence in a study on capillarization, the investigator is free to define either the total tissue, or the stroma as reference space. The former decision is the most natural and was chosen in Krasnoperov & Stoyan, (2004) and here. The latter choice makes the stereological investigation of capillaries somewhat more complicated. The estimation of second-order statistics such as $g(r)$ is then no more as straightforward as in this paper. In our investigation, the whole rectangular visual fields were used as the reference area. If only the stroma is taken as the reference area, the latter becomes a subset of the window of observation with irregular borders. In this case, it is not possible to use the simple edge correction by symmetrical minus-sampling to estimate $g(r)$ (border method; see e.g. Ripley, 1988). More refined edge-corrections, e.g. that one applied in this paper, must be used necessarily, when the stroma is used as the reference phase (Stoyan et al., 1995; Diggle, 2003). Concerning estimation of the first-order property L_V, we would have a ratio estimator with variable denominator, as the stromal fraction varies from field to

field within each case. This means that instead of taking the mean of ratios as done here, it would be necessary to sum up the number of capillaries over all fields and divide by the sum of the areas of the stroma of all fields, and to use a ratio-of-sums estimator. In this case similar statistical problems arise as in the case of volume fraction estimation from multiple fields with varying content of the reference phase per case using the Delesse principle (Mattfeldt & Fleischer, 2005). In the latter situation, using the ratio-of-sums estimator with variable reference area may, however, sometimes increase the precision. Whether the same holds for L_V of capillaries per unit stromal volume as compared to L_V of capillaries per unit tissue volume remains to be determined. Anyway, the conclusion that cancerous tissue in the prostate is more densely capillarized than normal tissue was not changed by this redefinition of the reference space for the present data. The estimated length of capillaries per unit stromal volume was found to be significantly enhanced in the carcinoma group also when the stroma was used as reference fraction ($p < 0.02$). The difference in favour of the neoplastic tissue even increased a little, as the stromal fraction in the neoplastic tissue tended to be lower than in normal tissue.

4.3 Discussion of various methodological aspects

In the present study, classical inference methods and bootstrap techniques were applied to compare mean reduced g-functions of two groups of cases. For this purpose, a pointwise, local approach (consecutive significance tests at all r-values), or a global approach (taking the whole series of $g(r)$-values into account simultaneously) are possible. In previous bootstrap studies on point process data, the global approach was used (Diggle et al., 1991, 2000; Schladitz et al., 2003). Thus, in the studies of Diggle and coworkers on brains of schizophrenic persons, the global question was addressed: do brains of schizophrenic persons and brains of normal persons differ spatially w.r.t. to various summary statistics of the point process of the neurons as seen in microscopic sections (Diggle et al., 1991, 2000)? In the present study, it was not only desired to find out whether the mean reduced g-functions for normal and neoplastic tissue differ globally, but at which specific ranges of interaction the significant differences emerge. Only the local approach gives an answer here. The global approach necessitates complex weighting procedures

(Diggle et al., 1991, 2000; Schladitz et al., 2003). Using the pointwise approach, it is possible to compute confidence intervals of reduced $g(r)$ for individual r-values, while the global approach would have let to a confidence band. Also we wanted to compare bootstrapping with classical tests; this is feasible with multiple t-tests as compared to multiple bootstrap tests, but a classical test alternative to the global test on significant difference between two functions is not obvious.

It might be argued critically that multiple tests on significant differences between group means for many r-values might lead randomly to falsely positive outcomes. If computer-intensive tests, such as randomization tests or bootstrap tests, are repeated many times with pairs of data sets from the same population, they will yield significant results in $\approx 5\%$ of the tests on average, if results are accepted as significant at the 5% level. This is a well-known problem of general statistics, for which such methods as the Bonferroni correction for multiple comparisons are available (Hsu, 1996; Sachs, 2003). For the present data, it was confirming to see that multiple t-tests and the bootstrap tests led to significant results in the same domains of r-values. Also, Table III shows that the rank of the bootstrap statistic and the t-statistic were roughly proportional. This result can hardly be ascribed to falsely significant outcomes by chance.

The main aim of the present paper was a comparison of capillary networks in normal prostatic tissue with capillary networks in prostatic cancer tissue in terms of the intensity and of the reduced g-function. In the first methodological paper (Krasnoperov & Stoyan, 2004), five laboratory animals have been investigated with one field per specimen at electron microscopy. Here we were confronted with human routine material, in which larger variability has to be expected. To increase the precision and to have an idea about the intraindividual variance 'within cases between fields', it was decided to evaluate not only one visual field, but two fields per case. Using the same workload, it would also have been possible to evaluate more small visual fields dispersed over the specimen. Probably this would have been the most efficient way towards estimation of L_V. However, here the estimation of the reduced g-function was the main concern and thus, the emphasis was put on few, comparatively large windows of observation. When it comes to the estimation of second-order statistics of point processes, the well-known motto 'Do more less well' (Gundersen & Østerby, 1981) is only of lim-

ited validity. Windows with smaller size may quickly attain a critical level of the numbers of points, in particular if the sizes of the windows are further diminished by minus-sampling. With too few points inside a window of observation, second-order statistics finally lose its sense (see e.g. Baddeley et al., 1993).

The present findings were compared to those of the first methodological paper (Krasnoperov & Stoyan, 2004). In general, both studies disclosed a hard-core effect in the initial parts of the g-functions, which was then followed by a domain of weaker repulsion. Thereafter the mean reduced g-function of the thyroid capillaries did not cut the reference line $g \equiv 1$ in the studied range of r-values (Krasnoperov & Stoyan, 2004, Fig. 6 therein). This happened however in the case of the prostate capillaries (Fig. 5). The reason may lie in the fact that in the EM study, the r-values ranged only from 0 to 40 μm, whereas here we used LM and evaluated higher values of r till 150 μm (Fig. 3). The estimated length density of capillaries was higher in the EM study, and a lower hard-core distance was found there (Krasnoperov & Stoyan, 2004). The two studies differ by the type of tissue, as well as by the microscopical methods (LM vs. EM resolution, thin vs. ultrathin sections). The estimate of r_0 amounted to ≈ 7.5 μm in (Krasnoperov & Stoyan, 2004, see Fig. 5 therein), whereas we found group mean values of 23–26 μm (Table I). At first sight it might appear contradictory that estimation of $g(r)$ using eqs. (2.16, 2.17) provided positive values for r-values distinctly below r_0 (see Table II). No interpoint distances can occur below the hard-core distance. However, when estimating $g(r)$ for stationary planar point processes, kernel methods should be used (Stoyan & Stoyan, 1994; Stoyan et al., 1995; Diggle, 2003; Baddeley & Turner, 2005). The application of any kernel leads to a smoothing of the g-values within the chosen bandwidth. This effect is also operative for the lowest values of r, and thus it fully explains the small positive values of $\widehat{g}(r)$ in the neighbouring region where $(r < r_0)$. In comparison to a previous investigation using immunohistochemistry and LM (Mattfeldt et al., 2004a), the estimated length densities of capillaries per unit tissue volume in the prostate were very similar. In general interactive detection of capillary profile centres is laborious. Nevertheless, it seems not utopic that the whole methodology shown in this LM study may become automated once in the future. Immunohistochemical staining can

be already performed automatically now, this holds also for the stain used in this study. With appropriate automatic segmentation, making use of the strong contrast of the stained capillaries to the remainder of the tissue, it seems not impossible that all capillaries may be correctly detected with image analysis software. However, as the present study was focused on research work, no attempts were yet made towards an adaptation of the method for high throughput in everyday routine.

When comparing bootstrap confidence intervals to classical confidence intervals, we found slightly wider intervals according to the bootstrap method (Table II). In our previous study on volume fractions (Mattfeldt & Fleischer, 2005), the bootstrap method provided narrower confidence intervals as compared to parametric bounds. This finding was explained as a result of a non-Gaussian distribution of the data in the previous study (Mattfeldt & Fleischer, 2005). For the present data set, the distribution of the $g(r)$-data between cases within groups appeared roughly consistent with a Gaussian distribution. Under this condition, it may well happen that the bootstrap method leads to less sharp confidence bounds, because a nonparametric technique is applied to data that essentially follow a Gaussian distribution. In general, bootstrapping is recommended nevertheless because of its robustness, as the compatibility of biological data with a Gaussian distribution is never granted *a priori.* Moreover, a useful side effect of the bootstrap method was found for low r-values, which led to very small g-values near 0 in both groups (see Table II for $r = 3$–6 pixels in the normal group and for $r = 3$–7 pixels in the carcinoma group). In these r-ranges, application of the parametric standard formula for computation of interval bounds led to negative lower bounds (Table II). However, these bounds make no sense for our g-functions, which assume only values ≥ 0. This finding may also be relevant for other applications, where confidence intervals for mean values of data sets with very small nonnegative values near 0 are desired. Clearly the method shown here is not the only approach for robust statistical inference from empirically estimated reduced g-functions. We restricted our evaluations to the classical version of the bootstrap, the so-called percentile method (Efron & Tibshirani, 1993; Ludbrook, 1995; Carpenter & Bithell, 2000). Other versions of the bootstrap are: the bootstrap-t-method, the bias-corrected method, and the bias-corrected and accelerated method; the reader is referred to the special literature

for details (Efron & Tibshirani, 1993; Ludbrook, 1995; Manly, 1997; Carpenter & Bithell, 2000). The percentile method seems to be the most popular one, is most easy to program and was also used by Diggle and coworkers in their analysis of spatial data (Diggle et al., 1991, 2000). A different computer-intensive approach consists in randomization tests, where resampling is performed without replacement (see e.g. Manly, 1997; Pitt & Kreutzweiser, 1998). Nonparametric rank tests, such as e.g. the Wilcoxon rank sum test, are also robust against vulnerations of the assumptions of normality and homoscedasticity (Sachs, 2003). Rank tests are not computer-intensive, easy to apply and can be found in most statistical standard packages. Regrettably randomization tests and rank sum tests can only be used for significance testing, but not for the computation of confidence intervals. However, the latter option is important in the context of second-order statistics, because the computation of confidence intervals allows to test the null hypothesis of absence of spatial correlation for a given distance. For this purpose, it may be checked whether the confidence interval of the reduced g-function at r includes the reference line $g \equiv 1$ (see Table II and Figs. 5a, b). This purpose can be achieved by parametric methods or bootstrapping, but not by randomization tests or rank tests.

Acknowledgments

Thanks are due to Gabriele Ehmke and Rolf Kunft for skilful technical assistance. Stefanie Eckel is supported by a grant of the graduate college 1100 at the University of Ulm.

References

Baddeley, A.J., Moyeed, R.A., Howard, C.V. & Boyde, A. (1993) Analysis of a three-dimensional point pattern with replication. Appl. Statist. 42, 641–668.

Baddeley, A. & Turner, R. (2005) spatstat: An R package for analyzing spatial point patterns. J. Statist. Software 12 (in press).

Cruz-Orive, L.M. (1989) Second-order stereology: estimation of second moment volume measures. Acta Stereol. 8, 641–646.

Diggle, P.J. (2003) Statistical Analysis of Spatial Point Patterns. Second edition. London: Arnold.

Diggle, P.J., Lange, N. & Beneš, F.M. (1991) Analysis of variance for replicated spatial point patterns in clinical neuroanatomy. J. Amer. Statist. Assn. 86, 618–625.

Diggle, P.J., Mateu, J. & Clough, H.E. (2000) A comparison between parametric and non-parametric approaches to the analysis of replicated spatial point patterns. Adv. Appl. Prob. 32, 331–343.

Efron, B. & Tibshirani, R.J. (1993) An Introduction to the Bootstrap. New York: Chapman & Hall.

Gundersen, H.J.G., Østerby, R. (1981) Optimizing sampling efficiency of stereological studies in biology: or "Do more less well!". J. Microsc. 121, 65–73.

Heimburg, S., Oehler, M.K., Papadopoulos, T., Caffier, H., Kristen, P. & Dietl, J. (1999) Prognostic relevance of the endothelial marker CD 34 in ovarian cancer. Anticancer Res. 19, 2527–2529.

Howard, C.V. & Reed, M.G. (2005) Unbiased Stereology. Three-Dimensional Measurement in Microscopy. Second edition. Oxford: Bios Scientific Publishers.

Hsu, J.C. (1996) Multiple Comparisons. Theory and Methods. London: Chapman & Hall.

Krasnoperov, R.A. & Stoyan, D. (2004) Second-order stereology of spatial fibre systems. J. Microsc. 216, 156–164.

Ludbrook, J. (1995) Issues in biomedical statistics: comparing means by computer-intensive tests. Aust. N. Z. J. Surg. 65, 812–819.

Manly, B.F.J. (1997) Randomization, Bootstrap and Monte Carlo Methods in Biology. Second edition. London: Chapman Hall.

Manwart, C., Torquato, S. & Hilfer, R. (2000) Stochastic reconstruction of sandstones. Phys. Rev. E 62, 893–899.

Mattfeldt, T. (2003) Classification of binary spatial textures using stochastic geometry, nonlinear deterministic analysis and artificial neural networks. Int. J. Pattern Recogn. Artif. Intell. 17, 275–300.

Mattfeldt, T. & Fleischer, F. (2005) Bootstrap methods for statistical inference from stereological estimates of volume fraction. J. Microsc. 218, 160–170.

Mattfeldt, T. & Mall, G. (1984) Estimation of length and surface of anisotropic capillaries. J. Microsc. 135, 181–190.

Mattfeldt, T. & Stoyan, D. (2000) Improved estimation of the pair correlation function. J. Microsc. 200, 158–173.

Mattfeldt, T., Mall, G., Gharehbaghi, H. & Möller, P. (1990) Estimation of surface area and length with the orientator. J. Microsc. 159, 301–317.

Mattfeldt, T., Frey, H. & Rose, C. (1993) Second-order stereology of benign and malignant alterations of the human mammary gland. J. Microsc. 171, 143–151.

Mattfeldt, T., Clarke, A. & Archenhold, G. (1994) Estimation of the directional distribution of spatial fibre processes using stereology and confocal scanning laser microscopy. J. Microsc. 173, 87–101.

Mattfeldt, T., Schmidt, V., Reepschläger, D., Rose, C. & Frey, H. (1996) Centred contact density functions for the statistical analysis of random sets. J. Microsc. 183, 158–169.

Mattfeldt, T., Gottfried, H.-W., Schmidt, V. & Kestler, H.A. (2000) Classification of spatial textures in benign and cancerous glandular tissues by stereology and stochastic geometry using artificial neural networks. J. Microsc. 198, 143–158.

Mattfeldt, T., Trijic, D., Gottfried, H.-W. & Kestler, H.A. (2004a) Incidental carcinoma of the prostate. Clinicopathological, stereological and immunohistochemical findings studied with logistic regression and self-organizing feature maps. BJU Intern. 93, 284–290.

Mattfeldt, T., Trijic, D., Gottfried, H.-W. & Kestler, H.A. (2004b) Classification of incidental carcinoma of the prostate using learning vector quantization and support vector machines. Cell. Oncol. 26, 45–55.

Mayer, J., Schmidt, V. & Schweiggert F. (2004) A unified simulation framework for spatial stochastic models. Simul. Modelling Pract. Theory 12, 307–26.

Pitt, D.G. & Kreutzweiser, D.P. (1998) Applications of computer-in-

tensive statistical methods to environmental research. Ecotoxicol. Environm. Safety 39, 78–97.

Ripley, B.D. (1988) Statistical Inference for Spatial Processes. Cambridge: Cambridge University Press.

Rubio, L., Burgos, J.S., Morera, C. & Vera-Sempere, F.J. (2000) Morphometric study of tumor angiogenesis as a new prognostic factor in nasopharyngeal carcinoma patients. Pathol. Oncol. Res. 6, 210-216.

Sachs, L. (2003) Angewandte Statistik. 11th edition. Berlin: Springer.

Schladitz, K., Särkkä, A., Pavenstädt, I., Haferkamp, O. & Mattfeldt, T. (2003) Statistical analysis of intramembranous particles using freeze fracture specimens. J. Microsc. 211, 137–153.

Stoyan, D. & Schnabel, H.-D. (1990) Description of relations between spatial variability of microstructure and mechanical strength of alumina ceramics. Ceramics Intern. 16, 11–18.

Stoyan, D. & Stoyan, H. (1994) Fractals, Random Shapes and Point Fields. Methods of Geometrical Statistics. Chichester: Wiley.

Stoyan, D., Kendall, W. S. & Mecke, J. (1995) Stochastic Geometry and Its Applications. 2nd edition. Chichester: Wiley.

Torquato, S. (2001) Random Heterogeneous Materials. New York: Springer.

Tscheschel, A. & Stoyan, D. (2005) Statistical reconstruction of random point patterns. Elsevier Science (conditionally accepted).

Vaquero, J., Zurita, M., Coca, S., Oya, S. & Morales, C. (2000) Prognostic significance of clinical and angiogenesis-related factors in low-grade oligodendrogliomas. Surg. Neurol. 54, 229–234.

Vidal, S., Kovacs, K., Horvath, E., Scheithauer, B.W., Kuroki, T. & Lloyd, R.V. (2001) Microvessel density in pituitary adenomas and carcinomas. Virchows Arch. 438, 595–602.

Weibel, E.R. (1979) Stereological Methods. I. Practical Methods for Biological Morphometry. London: Academic Press.

Yeong, C.L.Y. & Torquato, S. (1998) Reconstructing random media. Phys. Rev. E 57, 495–506.

Legends to the Tables

Table I. The summary characteristics are compared between the groups of tumour-free prostatic tissue and prostatic cancer tissue by means of Student's t-test. Abbreviations: N: number, $\bar{x}$: mean value, SD: standard deviation. For the other abbreviations see text.

Table II. The mean reduced g-functions are given r-wise with 95% confidence intervals for the tumour-free tissue group and for the prostatic cancer tissue group. In most instances, the bootstrap method yielded slightly wider intervals. Note negative lower bounds of parametric confidence intervals for mean values of g-functions at some low r-values in both groups. This effect was precluded by the bootstrap method.

Table III. The differences between the group mean values of $g(r)$ were tested locally for significance at fixed r-values. D= difference between sample means, BS = bootstrap sample. The asterisks indicate: $^{*}p < 0.05$, $^{**}p < 0.01$. Note slightly more conservative results according to bootstrap tests as compared to t-tests. Both approaches yielded evidence for differences with respect to interaction at two separate domains, see also Fig. 5c.

Table I. Group comparisons of summary characteristics

Estimate	Normal group		Cancer group		t	Level of significance
	$\bar{x}$	SD	$\bar{x}$	SD		
N(cap/field)	127	38	188	60	2.98	$p < 0.01$
L_V(cap/tiss) (mm/mm^3)	91.44	27.36	135.36	43.20	2.98	$p < 0.01$
r_0 (pixel)	17.33	4.51	15.33	4.02	1.62	N. S.
r_0 (μm)	26.00	6.77	23.00	6.03	1.62	N. S.
r_{max} (pixel)	26.77	6.18	30.75	12.32	1.41	N. S.
g_{max} (pixel)	1.41	0.29	1.10	0.24	3.83	$p < 0.001$
r_{min} (pixel)	40.68	8.53	40.12	16.22	0.15	N. S.
g_{min} (pixel)	1.02	0.20	0.94	0.21	1.38	N. S.
M	0.0279	0.0154	0.0139	0.0116	2.31	$p < 0.05$

Table II. Results of parametric and bootstrap methods
Comparison of 95%-confidence intervals

r	$\bar{g}(r)$	SD	parametric bounds	bootstrap bounds
Normal prostatic tissue				
3	0.0069	0.0239	−0.0083 0.0221	0.0000 0.0207
4	0.0115	0.0397	−0.0138 0.0367	0.0000 0.0458
5	0.0270	0.0609	−0.0117 0.0657	0.0000 0.0904
6	0.0574	0.0950	−0.0030 0.1178	0.0118 0.1235
7	0.1127	0.1458	0.0201 0.2053	0.0441 0.2054
8	0.1815	0.1887	0.0616 0.3014	0.0900 0.3021
9	0.2655	0.2071	0.1340 0.3971	0.1594 0.3853
10	0.3599	0.2152	0.2232 0.4967	0.2101 0.5264
20	1.1770	0.1909	1.0557 1.2984	1.0025 1.309
30	1.2738	0.2008	1.1463 1.4014	1.1542 1.4181
40	1.2106	0.1383	1.1227 1.2984	1.1177 1.3175
50	1.1616	0.1548	1.0633 1.2599	1.0491 1.2706
60	1.2049	0.1360	1.1185 1.2913	1.1072 1.3242
70	1.2099	0.1431	1.1190 1.3009	1.1029 1.3203
80	1.1846	0.1483	1.0904 1.2789	1.0832 1.3358
90	1.1633	0.1508	1.0674 1.2591	1.0456 1.2603
100	1.1377	0.1538	1.0400 1.2354	1.0264 1.2430
200	1.1093	0.0885	1.0531 1.1656	1.0526 1.1697
300	1.1002	0.0945	1.0402 1.1602	1.0373 1.1632
400	1.0117	0.1098	0.9419 1.0814	0.9284 1.1054
500	1.0256	0.0856	0.9712 1.0800	0.9568 1.1005
Prostatic cancer tissue				
3	0.0039	0.0093	−0.0020 0.0098	0.0000 0.0111
4	0.0109	0.0259	−0.0055 0.0273	0.0000 0.0344
5	0.0192	0.0383	−0.0052 0.0435	0.0000 0.0570
6	0.0262	0.0489	−0.0048 0.0573	0.0000 0.0648
7	0.0416	0.0673	−0.0011 0.0843	0.0043 0.0948
8	0.0636	0.0800	0.0128 0.1145	0.0130 0.1268
9	0.1053	0.0978	0.0431 0.1674	0.0438 0.1818
10	0.1656	0.1273	0.0847 0.2464	0.0864 0.2754
20	0.7493	0.3034	0.5565 0.9420	0.5542 1.0396
30	0.9551	0.2238	0.8129 1.0973	0.7903 1.1639
40	1.0704	0.1934	0.9475 1.1932	0.9327 1.2236
50	1.1092	0.1380	1.0215 1.1968	1.0101 1.2068
60	1.1058	0.0761	1.0574 1.1542	1.0533 1.1767
70	1.0793	0.1024	1.0142 1.1444	1.0039 1.1571
80	1.1055	0.1089	1.0363 1.1747	1.0202 1.1718
90	1.1354	0.1074	1.0672 1.2037	1.0606 1.2265
100	1.1027	0.0945	1.0427 1.1628	1.0340 1.1715
200	1.0606	0.0783	1.0109 1.1104	1.0112 1.1148
300	1.0251	0.0632	0.9850 1.0653	0.9804 1.0666
400	1.0732	0.0622	1.0336 1.1127	1.0323 1.1141
500	1.0123	0.0522	0.9791 1.0454	0.9781 1.0504

Table III. Group comparisons of g-functions
Parametric and bootstrap methods

r	Normal $\bar{g}(r)$	Cancer $\bar{g}(r)$	D	t	$P(t)$	Rank of D in 1000 BS
5	0.0270	0.0192	0.0078	0.38	0.7096	637
10	0.3599	0.1656	0.1944	2.69	0.0133	979*
15	0.8100	0.5019	0.3081	3.31	0.0032	979*
20	1.1770	0.7493	0.4278	4.13	0.0004	993*
25	1.3117	0.8715	0.4402	4.73	0.0001	998**
30	1.2738	0.9551	0.3187	3.67	0.0013	987*
35	1.2254	1.0206	0.2047	2.46	0.0223	951
40	1.2106	1.0704	0.1402	2.04	0.0532	957
45	1.1617	1.0978	0.0640	1.05	0.3047	828
50	1.1616	1.1092	0.0524	0.88	0.3906	764
55	1.1764	1.1237	0.0527	0.96	0.3473	758
60	1.2049	1.1058	0.0991	2.20	0.0384	958
65	1.2313	1.0943	0.1369	3.22	0.0039	991*
70	1.2099	1.0793	0.1306	2.57	0.0174	970
75	1.2149	1.0897	0.1252	2.41	0.0250	968
80	1.1846	1.1055	0.0792	1.49	0.1504	863
85	1.1689	1.1251	0.0437	0.77	0.4519	735
90	1.1633	1.1354	0.0278	0.52	0.6078	653
95	1.1682	1.1076	0.0606	1.06	0.3000	801
100	1.1377	1.1027	0.0350	0.67	0.5092	682
200	1.1093	1.0606	0.0487	1.43	0.1672	851
300	1.1002	1.0251	0.0750	2.29	0.0321	954
400	1.0117	1.0732	−0.0610	−1.69	0.1055	105
500	1.0256	1.0123	0.0133	0.46	0.6493	646

Legends to the Figures

Fig. 1. a) Tumour-free prostatic tissue from a radical prostatectomy specimen, removed because of prostatic cancer. Immunohistochemical stain with an antibody against the endothelial antigen CD34. Positively stained structures are visualized as brown dots. The capillaries lie within connective tissue (stroma). In the background one sees nonneoplastic prostatic glands with epithelial cells and lumina (white holes). **b)** The same image after detection of the centres of the capillary profiles. Note that many capillaries are located preferentially near the interfaces of epithelium and stroma, while another subset lies deeply within the stroma. The rectangular visual field consists of 1240 $\times$ 1000 pixels, which corresponds to 1860 $\mu m \times$ 1500 μm at the level of the specimen.

Fig. 2. a) Prostatic cancer tissue from a radical prostatectomy specimen, immunohistochemical CD34 stain as in Fig. 1. Here the epithelial component in the background consists of large neoplastic glands which often show a cribriform (sieve-like) pattern. **b)** The same image after detection of the centres of the capillary profiles. Note stromal septa which radiate into glands and contain capillaries.

Fig. 3. Selected visual field with 1240 $\times$ 1000 pixels. The crosses denote centres of capillary profiles.

Fig. 4. a) Estimated reduced g-function from a selected visual field of tumour-free prostatic tissue. Note hard-core effect in the beginning, then weaker repulsion, thereafter first maximum and first minimum. **b)** Estimated reduced g-function from a selected visual field of prostatic cancer tissue. Here the the curve ascends less steeply.

Fig. 5. a) Mean values and 95% confidence intervals for the reduced g-functions of the capillaries for tumour-free tissue. The confidence intervals were obtained r-wise by bootstrapping. **b)** Analogous plot for the prostatic carcinoma group. **c)** The mean reduced g-functions of the tumor-free group (continuous) and of the prostatic cancer group (stippled) are shown in superposition. The differences between the mean reduced g-functions are significant in the domains between r = 10–32 pixels and r = 64–69 pixels. In both regions the mean reduced g-function is diminished in the carcinoma group as compared to the normal tissue.

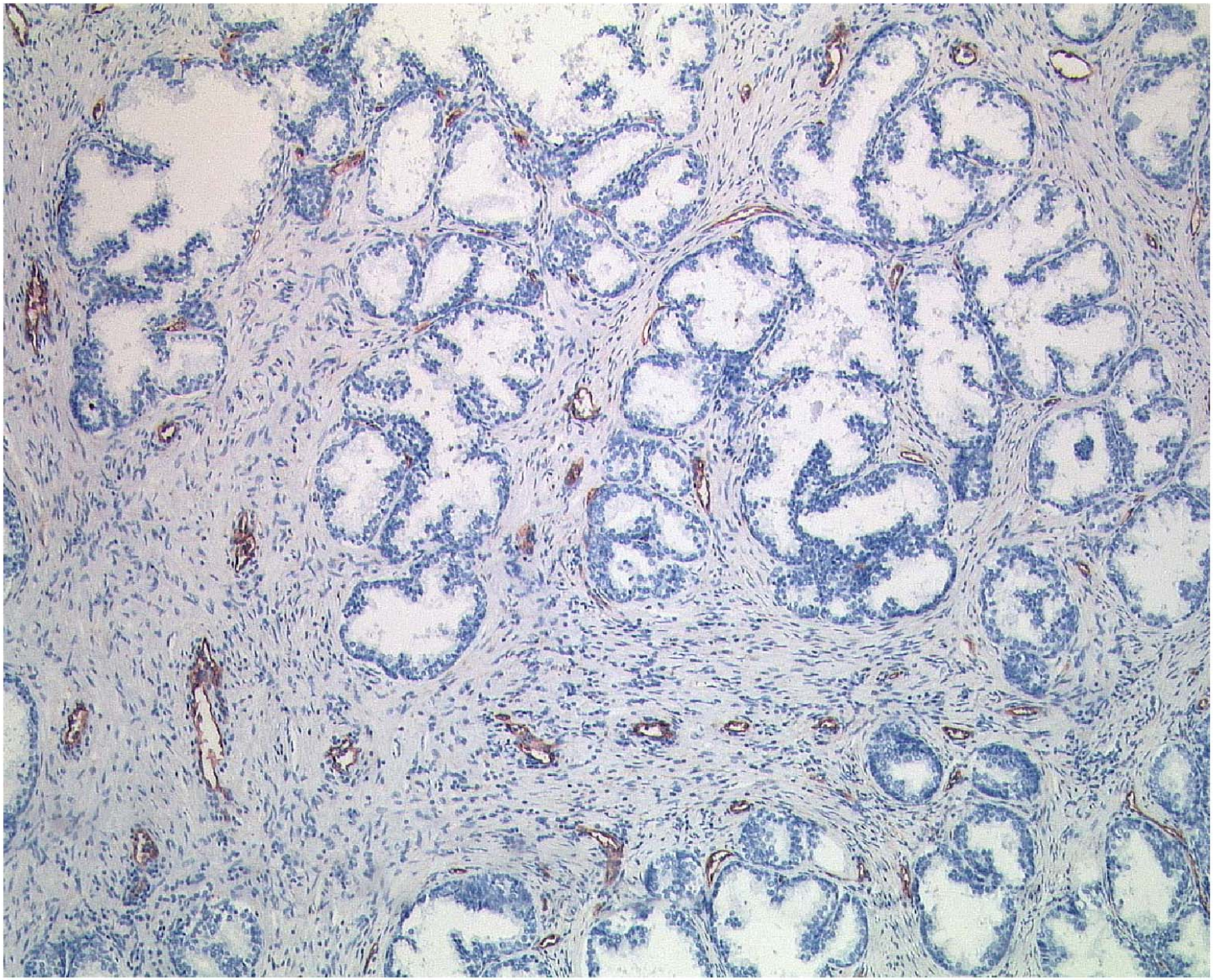

Fig. 1a

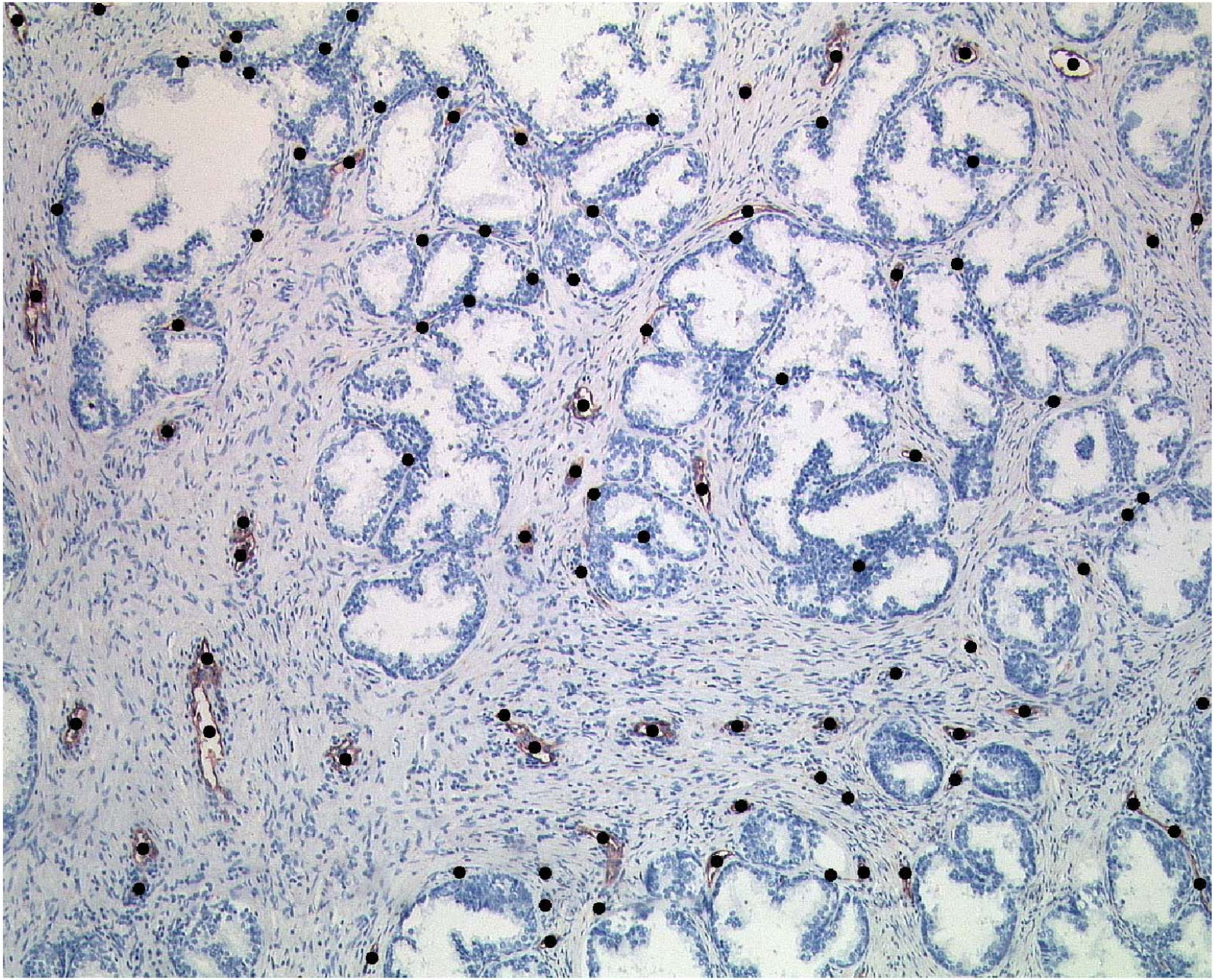

Fig. 1b

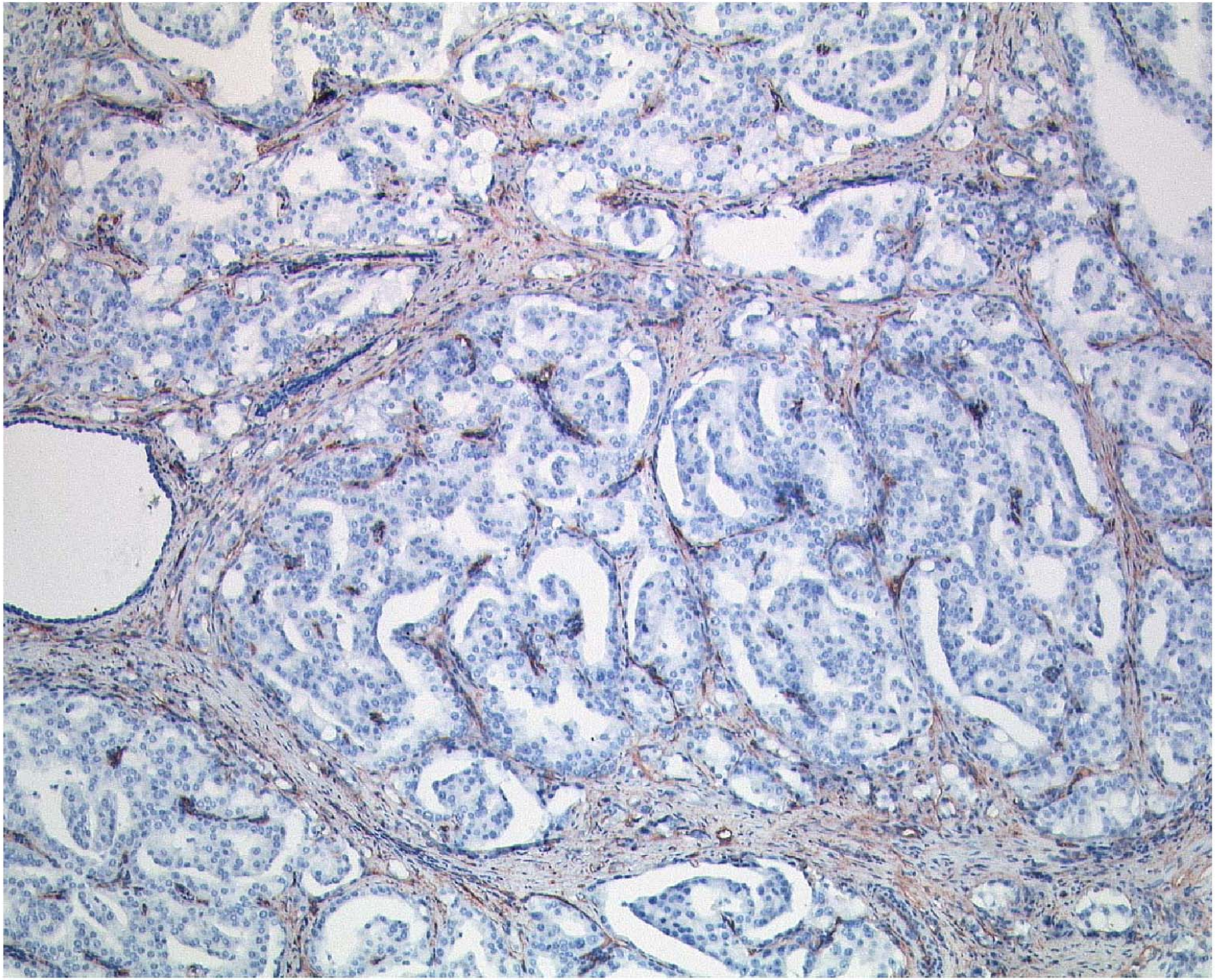

Fig. 2a

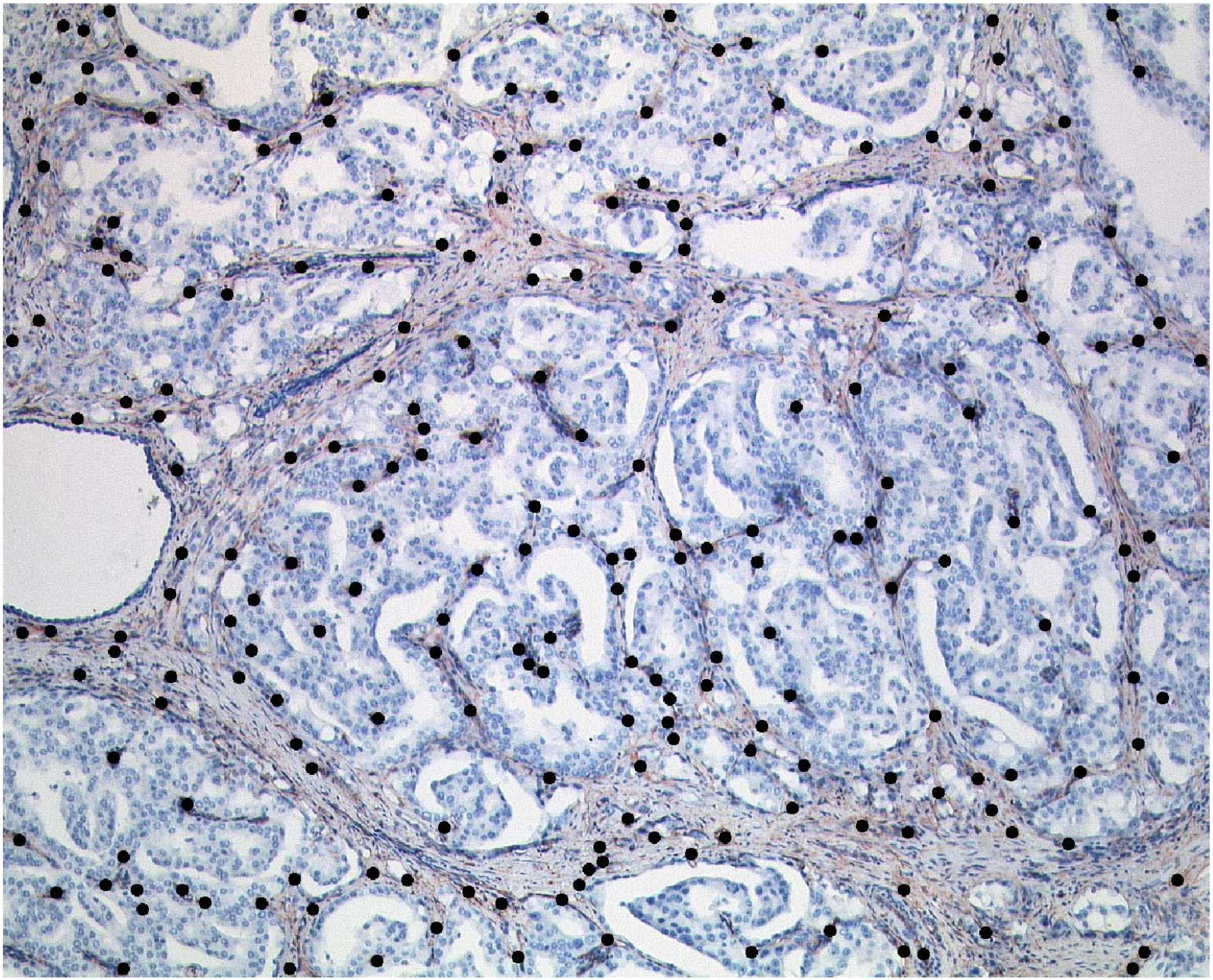

Fig. 2b

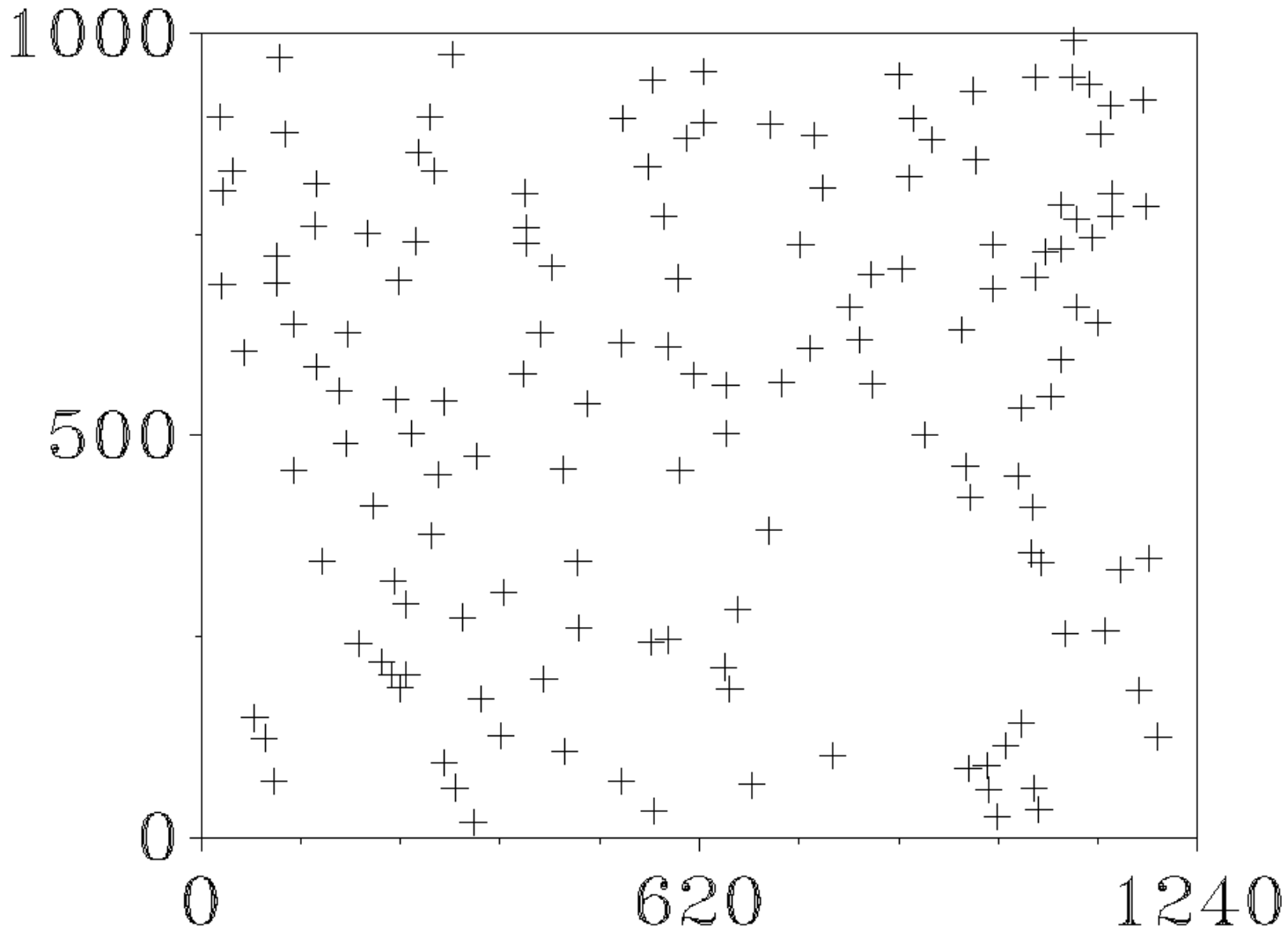

Fig. 3

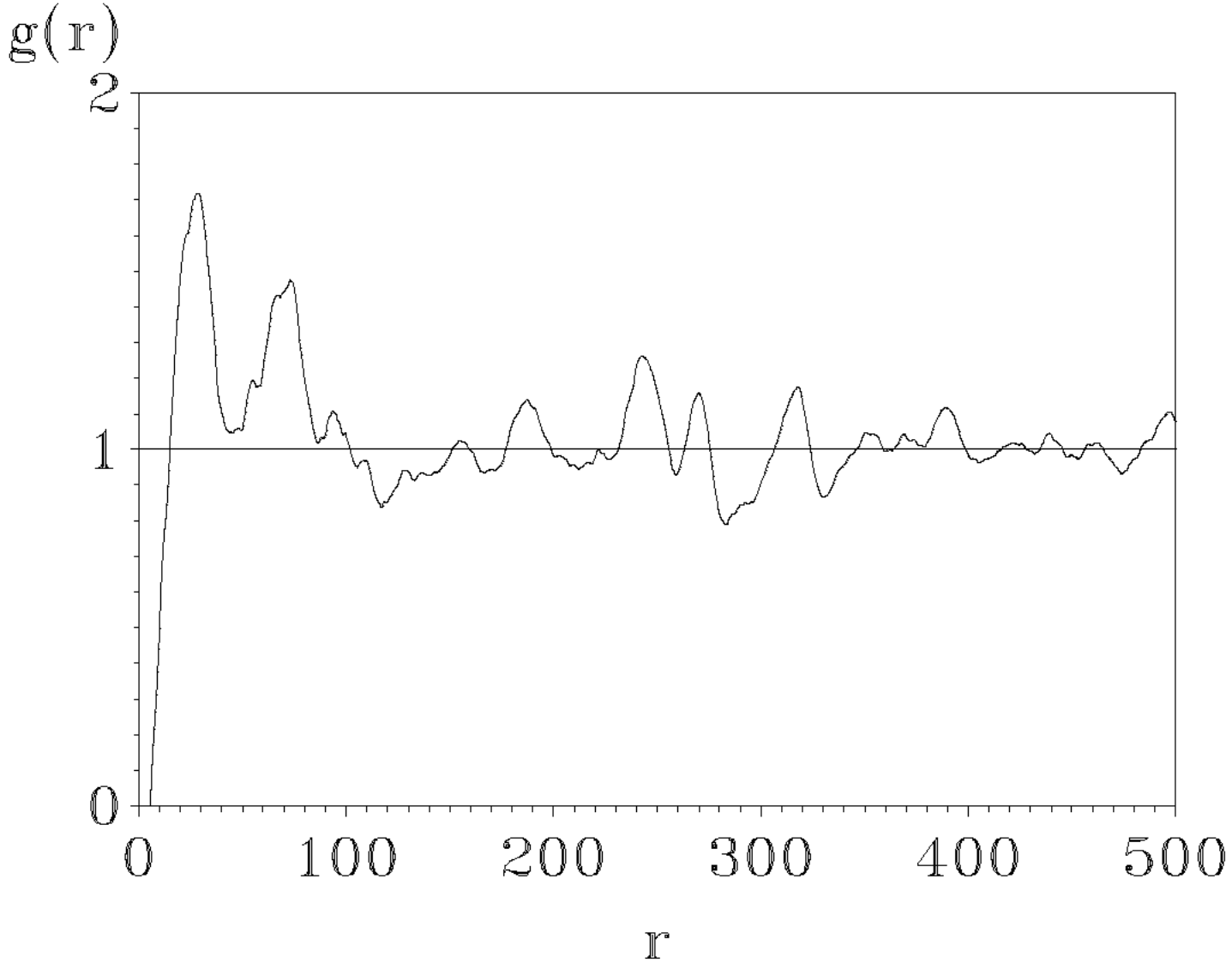

Fig. 4a

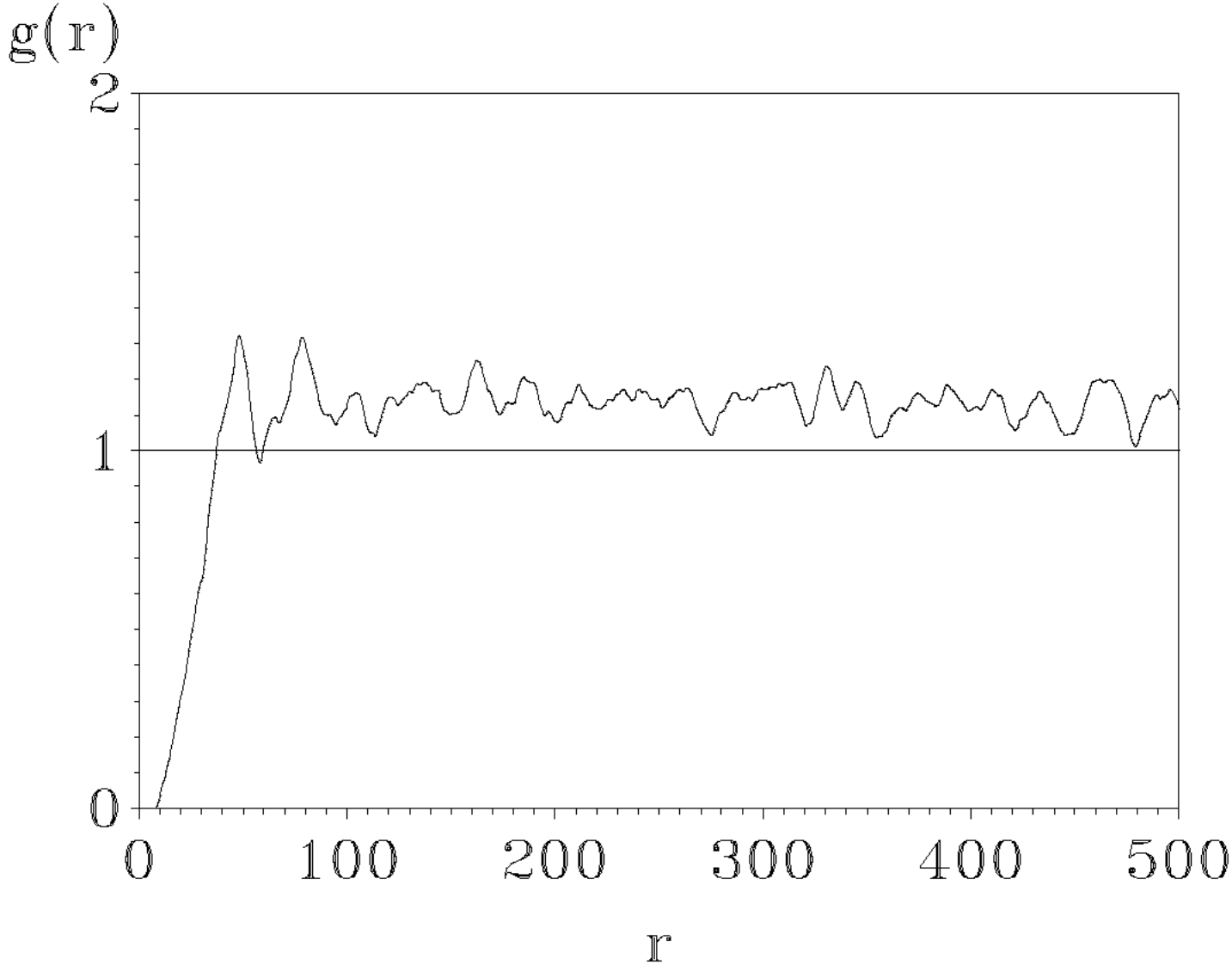

Fig. 4b

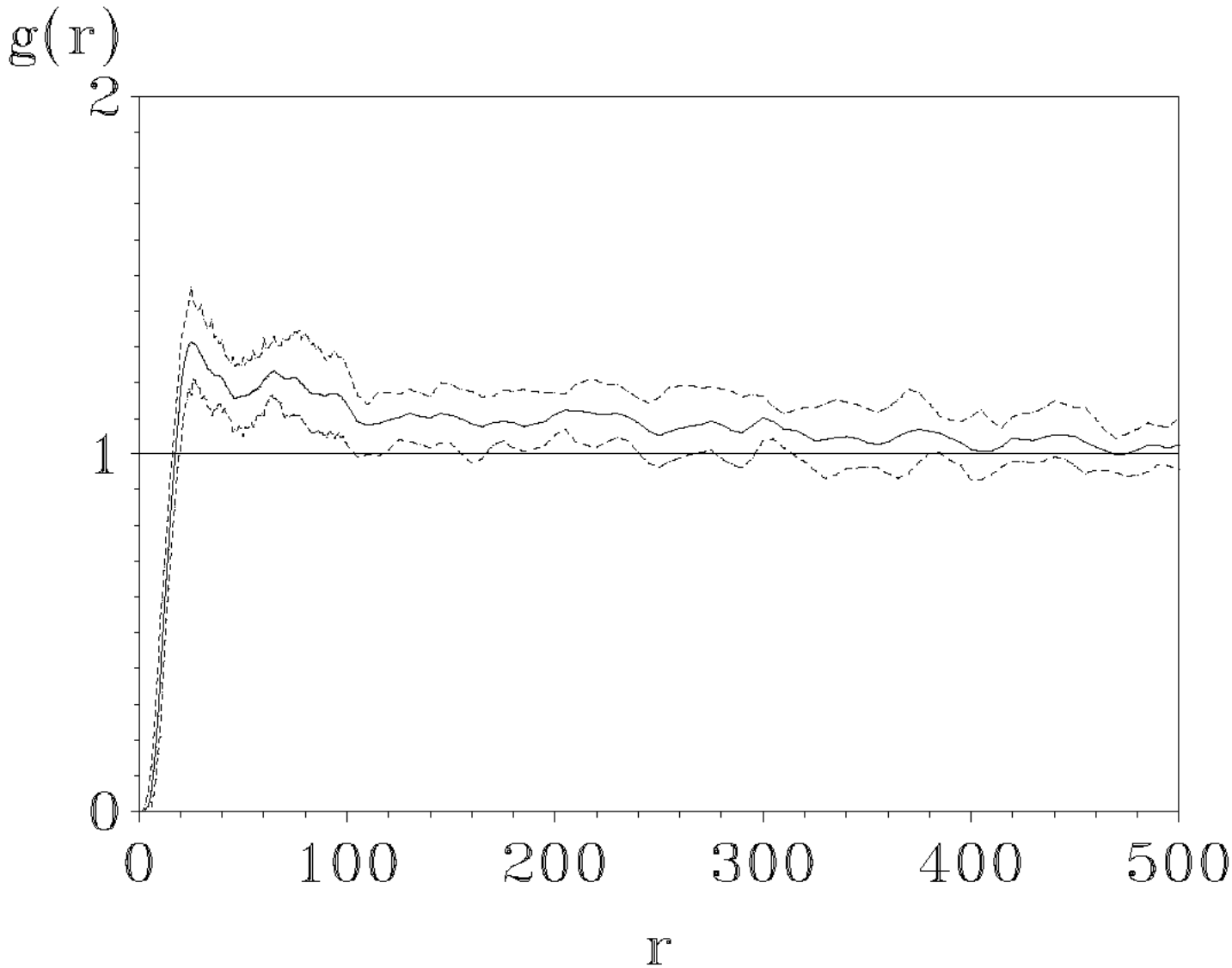

Fig. 5a

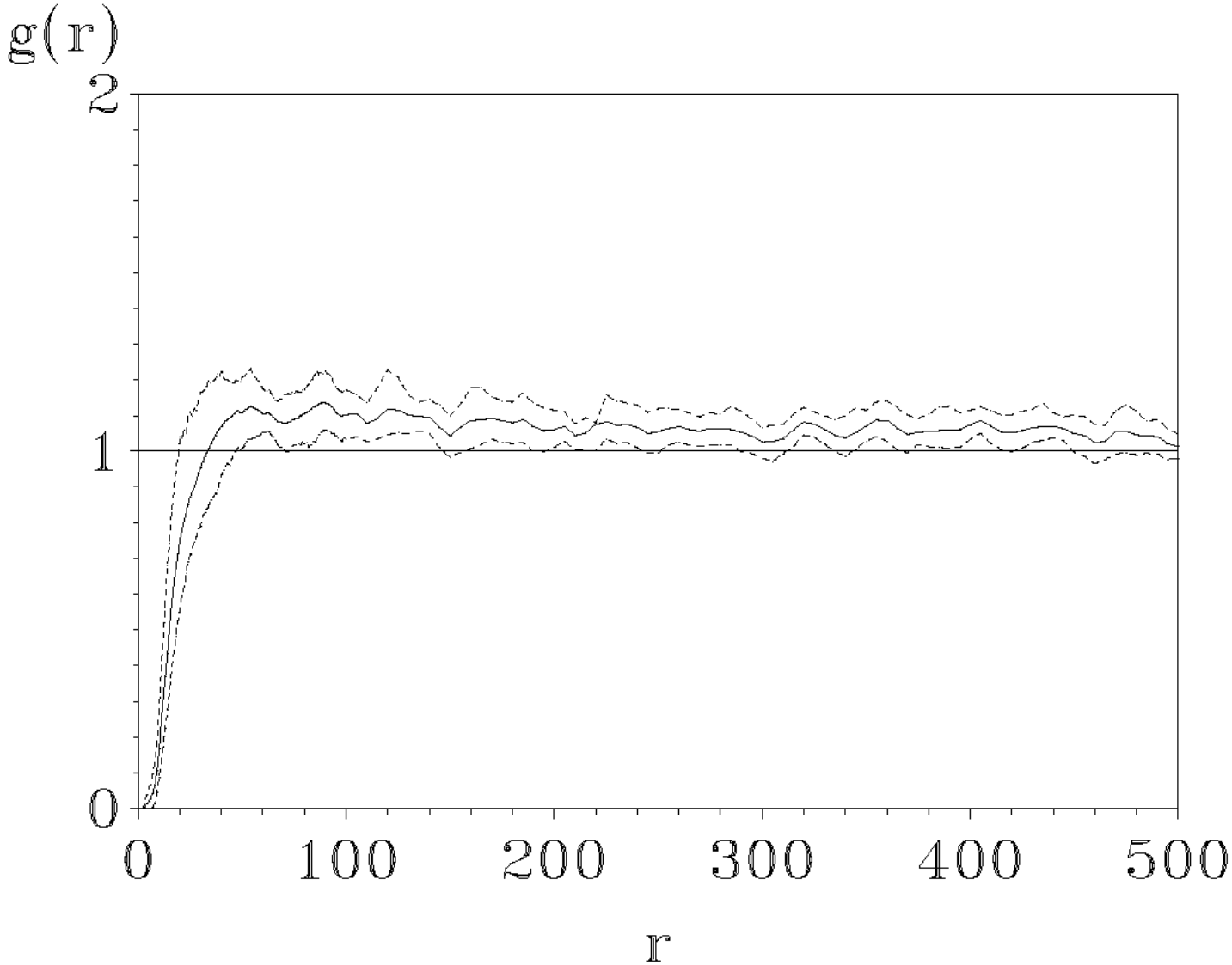

Fig. 5b

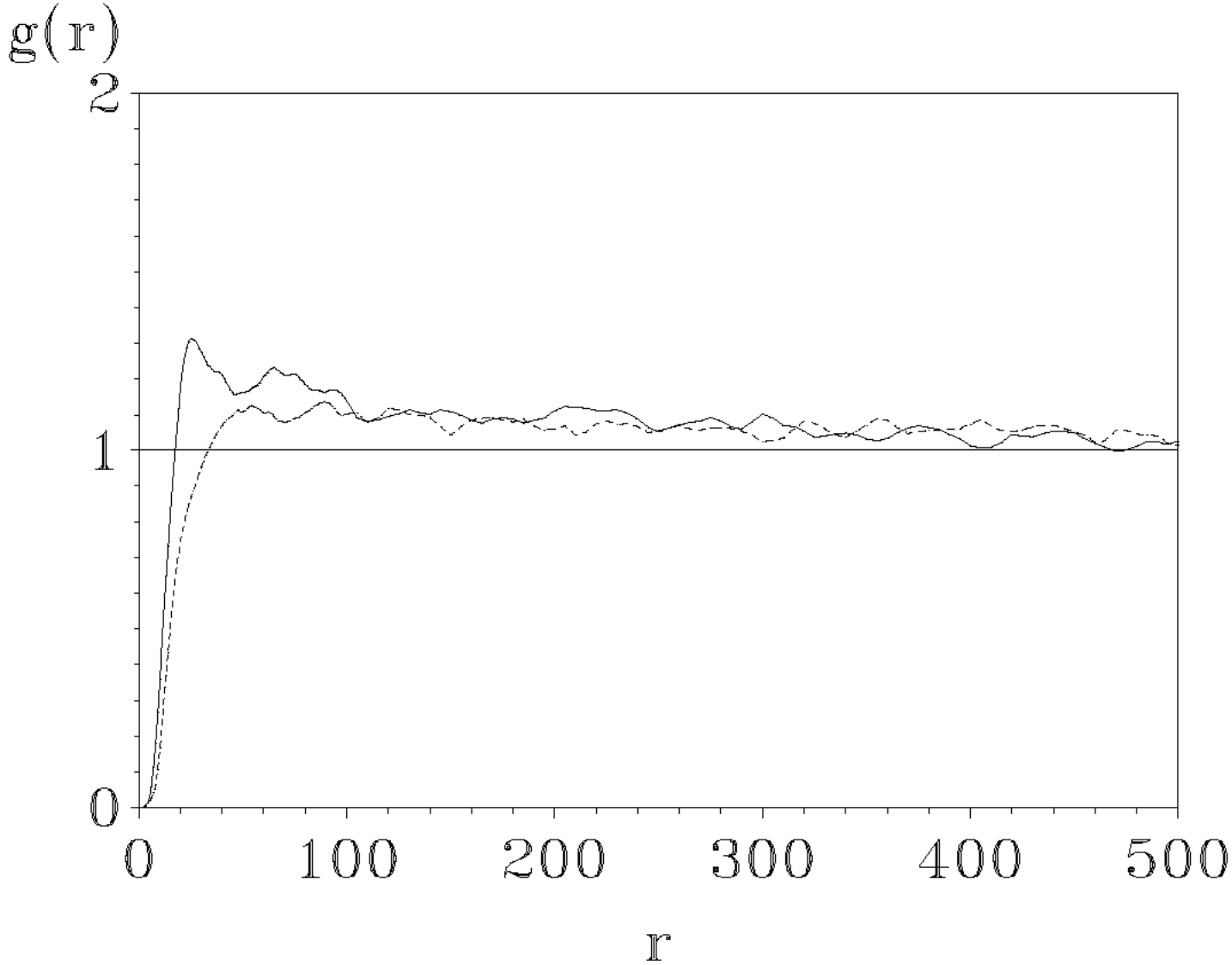

Fig. 5c